Case Studies in Construction Materials 16 (2022) e01110

Contents lists available at ScienceDirect

Case Studies in Construction Materials

journal homepage: www.elsevier.com/locate/cscm

Flexural behavior of UHPC beam reinforced with steel-FRP composite bars

Ebrahim M.A. Abbas [a], Yue Ge [b], Zhiwen Zhang [a], Yiwen Chen [a], Ashraf Ashour [c], Wenjie Ge [a,d,*], Rong Tang [a], Zhongping Yang [e], Ebrahim Y. Khailah [b], Shan Yao [e], Chuanzhi Sun [d]

[a] College of Civil Science and Engineering, Yangzhou University, Yangzhou 225127, China
[b] College of Hydraulic Science and Engineering, Yangzhou University, Yangzhou 225009, China
[c] School of Engineering, University of Bradford, Bradford BD7 1DP, UK
[d] Jiangsu Province Engineering Research Center of Prefabricated Building and Intelligent Construction, Suqian 223800, China
[e] Gansu Engineering Design Research Institute Co., LTD., Lanzhou 730030, China

ARTICLE INFO

Keywords:
Ultra-high performance concrete
Steel-FRP composite bar
Concrete beam
Flexural behavior

ABSTRACT

This paper numerically investigates flexural performance of Ultra-High Performance Concrete (UHPC) beam reinforced with Steel-Fibre-Reinforced Polymer (FRP) Composite Bars (SFCBs) in terms of flexural stiffness, moment capacity, deflection, ductility and energy dissipation. The effect of various parameters, include the inner steel core area ratio of SFCB, yield strength of inner steel core, elastic modulus and ultimate strength of outer-wrapped FRP, reinforcement ratio, type and strength of concrete were studied. The results demonstrate that the inner steel core area ratio of SFCB, reinforcement ratio and the elastic modulus of SFCB's outer FRP have significant effect on the overall flexural performance of SFCB reinforced UHPC beam. The overall flexural performance of SFCB reinforced UHPC beam is slightly improved by increasing the yield strength of inner steel core of SFCB, but not affected by the ultimate strength of SFCB's outer FRP when specimen occurred compression failure. The results also exhibit that the flexural performance of UHPC beam reinforced with SFCBs is significantly improved when compared to those of reinforced high strength concrete (HSC) beam and normal strength concrete (NSC) beam. The flexural stiffness and the moment capacity of SFCB reinforced UHPC beam at the ultimate point were 2.0 and 2.4 times, respectively, of those of reinforced NSC counterpart.

1. Introduction

Researchers have investigated the use of high strength steel in structural engineering applications [1,2]. However, the concrete beams reinforced with steel bars will be failed when the embedded steel bar is subjected to corrosion. Fibre-reinforced polymer (FRP) bar with characteristic of excellent corrosion resistance is considered as an efficient substitute for reinforcement steel to improve the durability of reinforced concrete structures in corrosive service environments [3–6]. However, FRP bar inherently has the characteristics of low elastic modulus and linear deformation until rupture, leading to large deflection, large cracks width and brittle failure. Fibre reinforced concrete is widely examined [7–13] to investigate the feasibility of using fibers to enhance the tensile strength as well as the toughness of concrete, decrease the development of deflection and cracks of reinforced concrete beam through its bridging

* Corresponding author at: College of Civil Science and Engineering, Yangzhou University, Yangzhou 225127, China.

https://doi.org/10.1016/j.cscm.2022.e01110
Received 22 January 2022; Received in revised form 13 April 2022; Accepted 25 April 2022
Available online 29 April 2022

effect. Abed et al. [3] investigated the effect of fibers types on Basalt FRP reinforced concrete beam. It is observed that adding fibers to concrete mixture increases the concrete ductility and restrains the cracks width. Al-Rousan et al. [14,15] investigated the effect of combined macro synthetic fibers and anchored Carbon FRP sheet on the performance of plain concrete beam. The tested results showed using the combination to improve the flexural performance as well as serviceability of the tested beam has a good efficiency.

A new Steel-Fibre-Reinforced Polymer (FRP) Composite Bar (SFCB) recently has been produced [16–20], which is composed of inner steel bar out-wrapped by FRP materials as shown in Fig. 1. The outer wrapped FRP can be one of basalt FRP (BFRP), glass FRP (GFRP), carbon FRP (CFRP) and aramid FRP (AFRP) material or even a hybrid FRP [21]. SFCBs have higher strength (compared to steel rebar), higher elastic modulus before yielding (compared to FRP rebar) and stable secondary stiffness after yielding according to test results under uniaxial and cyclic tensile loading tests [22]. All the tested studies on SFCBs reported that the stiffness of SFCB could be obtained based on the principle concept of composite material, which can be estimated according to the contribution of each part in parallel direction. In addition, SFCB has good ductility, and excellent corrosion resistance, which can combine the advantages of steel and FRPs bars as reinforcement in structural concrete members.

A few studies investigated the flexural performance of SFCBs reinforced concrete specimens. Ge et al. [23] and Sun et al. [24] conducted experimental studies on the flexural performance of concrete beams reinforced with SFCBs. Test results showed that SFCB-reinforced specimens had an improved stiffness, a higher cracking and yield load capacity, higher ductility, reduced crack width and smaller deflection as compared to FRP reinforced counterparts. In addition, a higher ultimate bearing capacity and a higher post-yield stiffness as compared to steel reinforced counterparts. Wang et al. [25] carried out an experiment on the flexural behavior of SFCB-reinforced coral aggregate concrete beams. Test results showed that the flexural stiffness enhanced, and the load-deflection relationship was approximately nonlinear. The rigidity of the beams were enhanced by around 20% by utilizing SFCBs. Ding et al. [26] found that SFCB RC members outperformed RC members in terms of stiffness, bearing capacity, and crack control ability. Zhou et al. [27] experimentally and theoretically investigated the flexural performance of SFCB reinforced sea-sand recycled concrete (SSRC) beams. It is reported that the deflection ductility of all SFCB reinforced SSRC beams is in between 3.7 and 4.9, and the ratio of peak load to yielding load ranged from 1.5 to 3.1, showing exceptional post-yield behavior.

SFCBs also perform a perfect bonding performance with different types of concrete. Experimental studies [21,28] on the bonding performance between SFCB and concrete, sea-sand concrete and coral aggregate concrete were conducted. It was concluded that SFCBs perform a perfect bonding performance with the previous mentioned concretes, and a good bonding durability in marine environment. In addition, Wang et al. [29] observed through experimental study that four stages, i.e. elastic, yield, peak and residual slip stages characterized bond-slip curves of the bond behavior between coral concrete beams and steel-CFRP bars. However, studies on the flexural performance of SFCB reinforced concrete specimens and the bonding performance of SFCB embedded in UHPC are still limited. As a result, further studies are needed in order to promote the usage of SFCBs in structural engineering applications.

UHPC has recently been produced as one of the modern cementitious material with ultra-high compression strength, high tensile strength, and excellent ductility. It was developed in response to a demand for higher-quality concrete. When compared to high performance concrete (HPC) and normal strength concrete (NSC), UHPC has unique properties such as a high binder content, fine aggregate size, fibre presence, and the use of a substantial quantity of super-plasticizers. UHPCs often contain fibres to improve their post-peak tensile strength behavior, ductility and energy absorption. Yoo et al. [10] found that steel fibres improved the post-peak behavior and ductility of reinforced Ultra-High Performance Fibre-Reinforced Concrete (UHPFRC) beams. Wille et al. [30], Allena and Newtson [31] investigated the mechanical properties of both plain and fibre reinforced UHPC mixtures, it was found that the compressive strength of steel fibre reinforced UHPC was higher than that of plain UHPC. In addition, the flexural strength of steel fibre reinforced UHPC was higher than that of plain UHPC.

The distributed fibers in UHPC mixture can also resist the shear force. Researchers [32–34] tested reinforced UHPC beams contain steel fibers and no stirrups. All the reported test results indicate that the shear strength of UHPC can be improved by using fibers. Pourbaba et al. [35] conducted an experimental study to investigate the flexural and shear behavior of UHPC beams and NSC beams under four point bending test. The results demonstrated that UHPC beams failed by bending while NSC beams failed by shear. Results also exhibited that the flexural and shear strength capacities of UHPC specimens were 3.5 times those of NSC counterparts.

Most of the reported studies on UHPC have been focused on the characterization of material properties, and a few experimental and analytical studies have been carried out on the flexural and shear behavior of UHPC members [36–39]. Ferrier et al. [40] reported that UHPFRC beam reinforced with FRP bars exhibited high load capacity when compared to that of counterpart reinforced with steel bars,

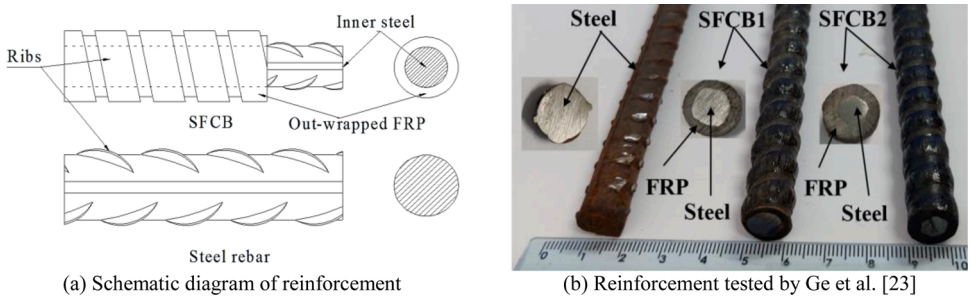

(a) Schematic diagram of reinforcement (b) Reinforcement tested by Ge et al. [23]

Fig. 1. Surface and cross-section comparison of SFCB and stee.

and presented typical behavior of reinforced concrete (RC) beam in tension or compression failure. Yoo et al. [41] found that the stiffness of FRP reinforced UHPFRC beams was significantly increased, and the crack width was significantly reduced, which solved the major shortcomings of ordinary FRP reinforced concrete beams. It was also found that UHPFRC beams reinforced with hybrid FRP and steel bars exhibited a higher post-cracking stiffness.

Simulation studies have become popular in most educational institutions around the world, particularly in engineering [42–46]. Some researchers used ABAQUS software by considering Concrete Damage Plasticity (CDP) model to conduct simulation studies on the flexural behavior of reinforced UHPC beam [47–50], but these studies are limited. Solhmirzaei et al. [47] used ABAQUS to solve the problem of a lack of numerical studies on the flexural behavior of UHPFRC beams and to assess the advantages of UHPFRC over NC. Shafieifar et al. [48] carried out an experimental study on small specimens to investigate the mechanical properties of UHPC and NC. In addition, a finite element numerical model considering (CDP) model was used to simulate the behavior of UHPC. The numerical modeling results were in good agreement with the experimental results. It was also found that the compressive and tensile strengths of UHPC were 3.0–4.0 times of those of NC, while the flexural strength was 4.5 times of that of NC.

Based on the literature review, it can be observed that most of the reported studies on SFCBs were focused on its mechanical properties and flexural behavior of SFCB reinforced NSC beams. While the effect of basic parameters such as the yield strength of inner steel core of SFCB, and the ultimate tensile strength and elastic modulus of SFCB's outer FRP materials on the flexural performance of SFCBs reinforced concrete beams is not clear. In addition, studies on flexural behavior of UHPC beams reinforced with steel bars, FRP bars, or hybrid FRP and steel bars are still limited, while flexural performance of UHPC beam reinforced with SFCBs has not been investigated yet. Accordingly, the first objective of this study is to combine SFCBs and UHPC in order to enhance the flexural behavior of SFCBs reinforced UHPC beams. The second objective is to investigate the effect of various parameters on the flexural performance of SFCBs reinforced UHPC beams in terms of flexural stiffness, moment capacity, deflection, ductility and energy dissipation. These parameters include the ultimate strength and elastic modulus of SFCB's outer FRP materials, yield strength of inner steel core, inner steel area ratio to the total area of SFCB cross-section, the SFCB reinforcement ratio, and strength and type of concrete. Therefore, a valid FE model of UHPC that obtained from the reference [48] was used to simulate reinforced UHPC beams, and three FE models were developed to simulate the flexural behavior of reinforced NSC and HSC beams, and were verified by the test results, in order to apply these models in the following parametric study. The mechanical properties of NSC and HSC were obtained from two different studies [23,51]; in addition, the mechanical properties of SFCBs were taken from the reference [23], while the mechanical parameters of UHPC model were obtained from the reference [48].

2. Description of specimens

Three tested beams under four-point bending test were selected to validate the developed models of NSC and HSC as well as SFCBs. The selected beams included: two SFCB-reinforced NSC beams tested by Ge et al. [23], and a steel-reinforced HSC beam tested by Lapko et al. [51]. Fig. 2 shows the size of the tested specimens, as well as their cross-sectional details. Table 1 presents the details of tested specimens. The NSC beam specimens had a 180 mm × 120 mm rectangular cross-section and a total span (L) of 1200 mm with effective span of 1080 mm and shear span (L_s) of 360 mm. The HSC beam specimen had a 200 mm × 120 mm rectangular cross-section, and a total span (L) of 3050 mm with effective span of 2950 mm and shear span (L_s) of 983 mm.

Two SFCB1 with diameter of 12 mm, three SFCB2 with diameter of 12 mm, and three steel bars with diameter of 16 mm were used as the longitudinal reinforcements of specimens N-SF1, N-SF2 and H-S1 beams, respectively. For the specimens N-SF1 and N-SF2, two

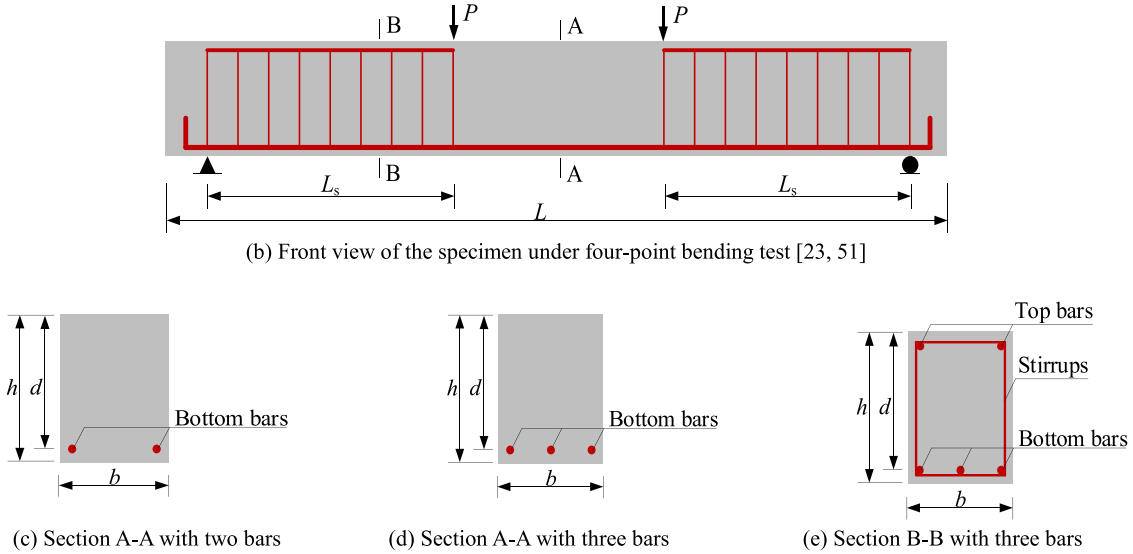

(b) Front view of the specimen under four-point bending test [23, 51]

(c) Section A-A with two bars

(d) Section A-A with three bars

(e) Section B-B with three bars

Fig. 2. Details of typical beam specimen.

Table 1
Details of the tested NSC and HSC beams.

NO.	$h \times b$ /mm	d/h	λ	ρ/ %	Bottom bars	Top bars	Stirrups
N-SF1	180 × 120	0.86	2.3	1.22	2 Φ 12	2 Φ 10	Φ 8 @ 90
N-SF2	180 × 120	0.86	2.3	1.82	3 Φ 12	2 Φ 10	Φ 8 @ 90
H-S1	200 × 120	0.84	5.85	3.0	3 Φ 16	2 Φ 10	Φ 6 @ 150

steel bars with diameter of 10 mm were adopted as erection reinforcement, and steel stirrups with diameter of 8 mm were distributed every 90 mm along the shear spans. For the specimen H-S1, two steel bars with diameter of 10 mm were adopted as erection reinforcement, and steel stirrups with diameter of 6 mm were distributed every 150 mm along the shear spans. Where the yield strength of erection bar and stirrup was 400 MPa. Where the reinforcement ratio $\rho = A_s/bd$, A_s is the reinforcement cross-section area, b is the beam width, and d is the effective height of section (distance from the compression zone fiber to the center of the bottom reinforcement bars), λ is the shear span ratio (ratio of the shear span to effective height of section). The labels N and H refer to NSC and HSC, the labels SF1 and SF2 refer to the SFCB1 and SFCB2, respectively; and S1 refers to steel materials with yield strength of 455 MPa.

3. Finite element model

Fig. 3 shows the typical details of the developed models for the beam specimens under four-point bending test. Firstly, three models were developed and analyzed to verify the validity of the models through a comparison between the simulation results and the tested results. After that, an FE model was established and analyzed to study the typical moment-deflection curve of UHPC beam reinforced with SFCBs, and twenty-three additional models to conduct parametric study. The designation of the NSC beam specimen was considered for the modeled specimens in the parametric study, where the width (b) and shear span (L_s) of the specimens were taken 0.1 and 0.3, respectively, of the total length (L) of specimens, and the effective height (d) was taken 0.86 of the total height of cross-section (h). Therefore, the beam with rectangular cross-section of 200 mm × 150 mm, and total length of 1500 mm was considered and modeled to conduct the parametric study. In addition, two steel bars with diameter of 12 mm were used as erection reinforcement, and steel stirrups with diameter of 8 mm were distributed every 50 mm along the shear spans.

3.1. Meshing and definition of the elements

Fig. 4 shows the effect of mesh size on the accuracy of simulated results. In order to ensure the convergence and accuracy of the FE model, and select the optimum mesh size to decreases the computational time, FE models were analyzed with three different mesh sizes ranging from coarse to fine mesh including 35, 25 and 15 mm. It is observed that the difference in accuracy between mesh sizes of 15 mm and 25 mm is very small. For UHPC model. It was observed that the difference in accuracy of simulated results between mesh sizes of 15 and 25 mm was very small [48]. Therefore, FE models were meshed using elements with dimensions no more than 25 mm. The mesh size of 15 mm was selected to show the cracks pattern clearly.

The concrete element and steel plates were simulated via solid element C3D8R available in ABAQUS software. The element C3D8R is an 8-nodes linear brick element with reduced integration. The meshing of solid elements is shown in Fig. 3. The stiffness of SFCB can be obtained based on the principle concept of composite material, as reported and adopted in the experimental studies [18,22,23]. Therefore, the reinforcement elements, which include bottom and erection bars, and stirrups were simulated by T3D2 element. The T3D2 element is a 2-nodes linear displacement element, and each node has three translational degrees of freedom.

3.2. Material properties

3.2.1. Concrete

The mechanical properties of UHPC, HSC and NSC were obtained from the experimental studies [48], [51] and [23], respectively. The cubic compressive strength of NSC was 43.85 MPa, which equivalent the concrete grade C45 according to Europe Code specifications [52]. While HSC mix was designed to obtain the mechanical properties of the concrete grade C105, where the test results of the cubic compressive strength and split tensile strength were 115.4 and 6.2 MPa, respectively. Therefore, the two concrete grades, C45

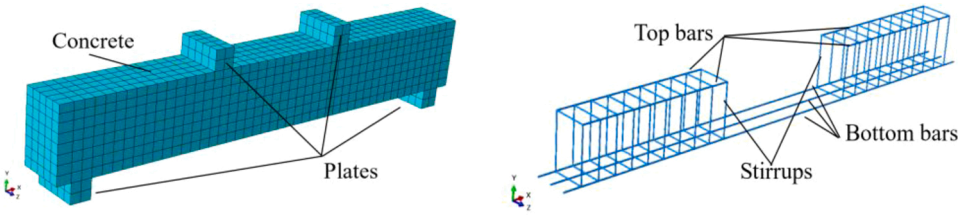

`(a) Model of concrete and loading plates (b) Model of reinforcement

Fig. 3. Typical geometry of FE model.

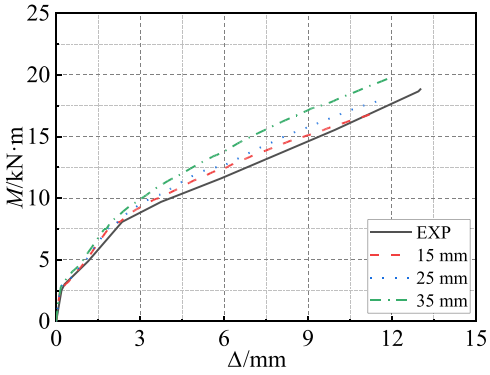

Fig. 4. Sensitivity analysis of N-SF1 grid size.

and C105, were adopted to represent NSC and HSC, respectively. The mechanical properties of UHPC were obtained based on various conducted experimental tests [48] to determine the compressive strength, tensile strength, and modulus of elasticity of UHPC.

Table 2 lists the mechanical properties of UHPC in terms of compressive strength (f_c), tensile strength (f_t), elastic modulus (E_c), and Poisson ratio (ν).

Table 3 lists the mechanical properties of the two concrete grades investigated in terms of mean compressive strength (f_{cm}), tensile strength ($f_{tk,0.05}$), mean elastic modulus (E_{cm}), Poisson ratio (ν), strain corresponding to peak stress (ε_{cp}), and strain corresponding to ultimate stress (ε_u) according to Europe Code specifications [52].

In reference [51], the design rules and the compression stress-strain relationship of concrete, which are proposed by EC2 [52], were used to define the nonlinear behavior of NSC and HSC under compression. Therefore, this relationship was adopted in the present study, which can be expressed as follows.

$$\frac{\sigma_c}{f_{cm}} = \frac{k\eta - \eta^2}{1 + (k-2)\eta} \qquad \varepsilon_c \le \varepsilon_{cu} \tag{1}$$

The tension stress-strain relationship of concrete which developed by Massicotte et al. [53] was adopted to define the nonlinear behavior of NSC and HSC under tension. This relationship assumes that the post-peak tensile stress is reduced by 66.7% at a strain of about 5 times the strain at first cracking. Then reduced to zero at a total strain of about 16 times the strain at first cracking. For UHPC, the compression and tension stress-strain relationship were calculated and drawn using the Eqs. (2, 3) according to the stress-inelastic strain data in Table 5. Fig. 5 shows the stress-strain relationship of each concrete type in compression and tension behavior. Where $\eta = \varepsilon_c/\varepsilon_{cp}$, $k = 1.05E_{cm}\varepsilon_{cp}/f_{cm}$, f_{cm} is the mean compressive strength of concrete, σ_c is the compressive stress of concrete, ε_c is the compression strain of concrete, ε_{cp} is the strain of concrete at the maximum stress, E_c is the secant modulus of elasticity of concrete, and ε_{cu} is the ultimate compression strain of concrete. $f_{ctk;0.05}$ is the peak tensile strength of concrete with 5% fractile.

Table 4 shows the parameters of CDP model for the three types of concrete. Where the parameters of CDP model for NSC and HSC were proposed based on the adopted values in references [43,54]. Whereas all the parameters of CDP model for UHPC were obtained from reference [48].

Table 5 shows the stress-inelastic strain data of UHPC [48]. The stress data of concrete under tension and compression behavior at plastic stage are defined as a tabular function of cracking strain (ε^{ck}), and inelastic strain (ε^{in}) respectively, which can be expressed as follows [54].

$$\varepsilon^{in} = \varepsilon_c - \sigma_c/E_c \tag{2}$$

$$\varepsilon^{ck} = \varepsilon_t - \sigma_t/E_c \tag{3}$$

After the stress reaches the peak tensile stress of concrete material, the tensile damage parameter d_t is provided as a tabular function of cracking strain, which can be expressed as follows [43,48].

$$d_t = \begin{cases} 0 & \sigma_t \le \sigma_{tmax} \\ 1 - \sigma_t/\sigma_{tmax} & \sigma_t > \sigma_{tmax} \end{cases} \tag{4}$$

For NSC and HSC, the compressive damage parameter d_c is provided as a tabular function of crushing strain, which can be calculated by the Eq. (5) [43]. For UHPC, the compressive damage parameter - in the original source for all CDP parameters for UHPC

Table 2
Mechanical properties of UHPC [48].

Material	f_c /MPa	f_t /MPa	E_c /GPa	Poisson's ratio
UHPC	138	9.7	54.7	0.18

Table 3
Mechanical properties of the two concrete grades [52].

Concrete grade	$f_{cu,k}$/MPa	f_{cm}/MPa	$f_{ctk,0.05}$/MPa	E_{cm}/GPa	ε_{cp}	ε_{cu}	Poisson's ratio
C45	45	43	2.2	34.0	0.00225	0.0035	0.2
C105	105	98	3.5	52.0	0.0028	0.0028	0.2

Table 4
Parameters of concrete damage plasticity model (CDP).

Material	Dilation angle (ψ)	Eccentricity	Stress ratio (f_{b0}/f_{c0})	Shape factor (k)	Viscosity Parameter
NSC, HSC	31	0.1	1.16	0.66	0.0001
UHPC	56	0.1	1.16	0.66	0.00

Table 5
The stress-inelastic strain data of UHPC [48].

Compressive behavior		Tensile behavior	
Compressive stress/MPa	Inelastic strain	Tensile stress/MPa	Cracking strain
124	0	0.7	0
138	0.001	9.7	0.0035
76	0.009	2.1	0.0500

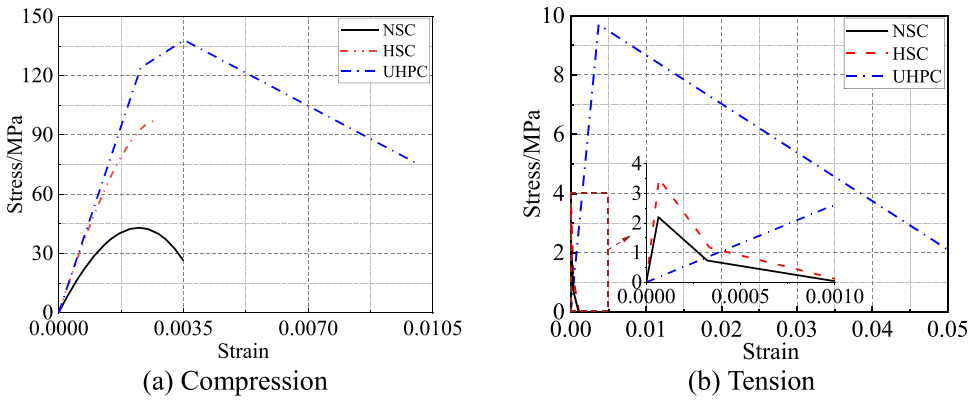

Fig. 5. Stress-strain relationship of NSC, HSC and UHPC.

[48] was not included in the CDP model. Similarity, due to the high compressive strength and linear behavior of UHPC until its peak compressive stress, the compressive damage parameter was not included in the CDP model [47,55]. Where σ_t and σ_c are the tensile and compressive stress in concrete, respectively, σ_{tmax} and σ_{cmax} are the maximum tensile and compressive stress of concrete, respectively, and ε_t and ε_c are the tensile and compressive strain in concrete, respectively.

$$d_c = \begin{cases} 0 & \sigma_c \le \sigma_{cmax} \\ 1 - \sigma_c/\sigma_{cmax} & \sigma_c \ge \sigma_{cmax} \end{cases} \tag{5}$$

3.2.2. Reinforcements

The tensile properties of SFCBs are listed in Table 6. The tensile properties of SFCBs were obtained from the results tested by Ge et. al [23], and Poisson's ratio (ν) of 0.3 was adopted for all reinforcement bars.

Fig. 6 presents the stress-strain relationship of reinforcements. The nominal stress-strain relationship of SFCB can be expressed as follows [23]. Where ε_{sf} and f_{sf} are the tensile strain and corresponding stress of SFCB, respectively, ($E_1 = \alpha_s E_s + \alpha_f E_f$) is the modulus of

Table 6
Mechanical properties of SFCBs.

Material	Diameter/mm	Yield Strength/MPa	Ultimate strength/MPa	Modulus of elasticity E_1/GPa	Secondary stiffness E_2/GPa
SFCB1	12	230.0	704.0	113.0	30.6
SFCB2	12	150.2	798.5	72.3	25.7

elasticity of SFCB, and ($E_2 = \alpha_f E_f$) is the stiffness of SFCB after yielding of inner steel. f_{sfy} and f_{sfu} are the yield and ultimate strength of SFCB, respectively, ε_{sfy} is the yield strain of inner steel core, and ε_{sfu} is the ultimate tensile strain of out-wrapped FRP. α_s and α_f are the inner steel core area ratio and the outer FRP area ratio to the total area of SFCB, respectively, and E_s and E_f are the modulus of elasticity of inner steel and outer FRP, respectively.

$$f_{sf} = \begin{cases} E_1 \varepsilon_{sf} & 0 < \varepsilon_{sf} \le \varepsilon_{sfy} \\ f_{sfy} + E_2(\varepsilon_{sf} - \varepsilon_{sfy}) & \varepsilon_{sfy} < \varepsilon_{sf} \le \varepsilon_{sfu} \end{cases} \tag{6}$$

The nominal stress-strain relationship of steel can be expressed as follows [23]. where ε_s and f_s are the tensile strain and the corresponding stress of steel, and ε_{sy} and ε_{su} are the yield and ultimate strain of steel.

$$f_s = \begin{cases} E_s \varepsilon_s & \varepsilon_s \le \varepsilon_{sy} \\ f_{sf} & \varepsilon_s > \varepsilon_{sy} \end{cases} \tag{7}$$

The reinforcement steel was modeled as a bilinear elastic-perfect plastic material, and the SFCB reinforcement was modeled as a bilinear elastic-plastic material using the true stress-strain relationship. The true stress, strain and plastic strain of reinforcement bar can be expressed as follows [54]. where σ^t and σ_{nom} are the true and nominal stress of reinforcement respectively, ε^t and ε_{nom} are the true and nominal strain of reinforcement respectively, ε^{pl} is the plastic strain of reinforcement, and E is the elastic modulus of reinforcement.

$$\sigma^t = \sigma_{norm}(1 + \varepsilon_{norm}) \tag{8}$$

$$\varepsilon^t = \ln(1 + \varepsilon_{norm}) \tag{9}$$

$$\varepsilon^{pl} = \varepsilon^t - \sigma^t / E \tag{10}$$

3.3. Interactions and boundary conditions

All specimens were modeled as simply supported beams, where the translational displacements in the Y and Z directions were restrained by a roller support, and the transitional displacements in the X, Y and Z directions were restrained by a pinned support, which were defined to the middle line of bottom surface of the support plate along the Z-direction. The support and loading plates were placed at the corresponding loading point and end supports to avoid stress concentration, and were simulated with material properties of steel. Reference points were set at the center of the top surface of loading plates, and were "coupled" with the corresponding surface. The loading process was applied to the reference points consisted of an axial displacement with a maximum increment of 0.05 mm. “Tie” contact was adopted for the contact between the steel plates and specimen, while the “embed” technique was used to define the bond behavior between reinforcement bars and concrete as a perfect bond.

4. Model verification

The selected specimens described in the preceding section were modeled and evaluated in order to validate the accuracy of the developed numerical models. The comparison of predicted and experimental results of moment-deflection curve, moment capacities and its corresponding deflections in terms of cracking, yielding and ultimate moment (M_c, M_y and M_u), cracking, yielding and ultimate deflection (Δ_c, Δ_y and Δ_u), cracks pattern and failure mode were illustrated in the following subsections.

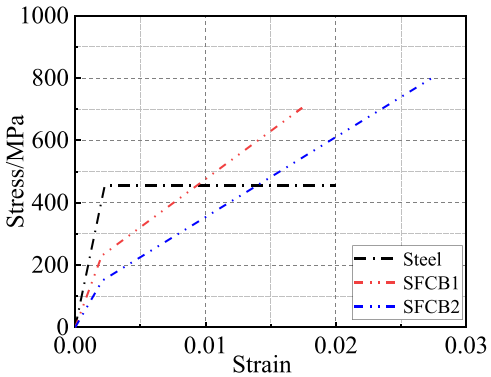

Fig. 6. Nominal stress-strain relationship of reinforcement bars.

4.1. Moment-deflection curves

The numerical moment-deflection curves were compared with the test results as shown in Fig. 7. It can be seen that the FE modeling curves had good agreement with the experimental curves for all the stages of the loading process. In addition, the overall trend for the moment-deflection curves were also reproduced well by the FE model for all the selected beams specimens. However, the initial stiffness of N-SF1 and N-SF2 specimens from the simulation results was higher than that from the test results, and the peak load of all beams specimens were considerably underestimated by the FE simulation. These results can be attributed to the difference between the modeling and testing boundary conditions. For H-S1 specimens, only the moment-deflection curve for the initial stage and post-cracking stage of loading process until yield of reinforcement steel bars were compared according to the available test data.

4.2. Moment capacity and its corresponding deflection

To further demonstrate the validity of the developed FE model, the moment capacities and its corresponding deflections of the selected beams were compared with the corresponding experimental results as listed in Tables 7 and 8. Where the Average Percentage Error (*APE*) of simulation to experimental results, and the Standard Deviation (*SD*) values were calculated and compared.

From Table 7, it was found that the average percentage error of simulated cracking, yield and ultimate moments were 0.12, 0.03 and 0.06, respectively. For specimen H-S1, it was found from the experimental results that the moment capacities corresponding to the deflection values of 9.0 and 13.5 mm were 22.1 and 31.95 kN.m, respectively [51]. While from the simulation results, it was found to be 22.6 and 31.5 kN·m, respectively, with average simulation to experimental results ratios of 1.02 and 0.98, respectively.

From Table 8, it was found that the average percentage error of simulated yield and ultimate deflection values were 0.097 and 0.095, while the cracking deflection values from the test results for N-SF1 and N-SF2 specimens were about two times the values from the simulation results. However, the deference in value was less than 0.25 mm.

Overall, the moment capacities and its corresponding deflections from FE simulation results were in good agreement with the tested results, indicating the validity of the developed models.

4.3. Cracks pattern

Fig. 8 shows the comparison of typical cracks pattern of specimens N-SF1 and N-SF2 at failure state. The cracks propagation in the tensile region of specimens N-SF1 and N-SF2 from the simulation results is similar with the experimental results, where several vertical cracks and a few inclined cracks developed and propagated. In addition, the concrete crushing failure occurred at both the experimental and simulation tests. Overall, the region of tension-damaged concrete from the FE model is consistent well with that from the experimental test, indicating that the developed FE models can well predict the propagation and pattern of cracks.

5. Moment-deflection curve of SFCBs reinforced UHPC beams

Fig. 9 shows the typical moment-deflection curve of SFCBs reinforced UHPC beams. A FE model was developed to simulate the moment-deflection curve of UHPC beams reinforced with SFCBs. The specimen size and its reinforcement details used were the same as those described in Section 3. According to analysis results, the moment-deflection curve of the SFCBs reinforced UHPC beam mainly consists of three stages (see Fig. 9): 1) First stage (elastic stage, initial point–A): form the initial loading to the SFCBs yielding. In this stage, both the concrete and SFCBs are in the elastic stage resulted in a linear relationship between moment capacity and its corresponding deflection, because UHPC in this study presents linear response until its peak tensile stress at a strain of larger than the SFCBs yielding strain according to the test results in the reference [2,48] Second stage (A–B): after the yielding of inner steel core of SFCBs until UHPC reaches its peak tensile stress. In this stage, although the inner steel core of SFCB reaches its yield strain, the flexural stiffness of specimen slightly decreases, because UHPC is still in the elastic stage, and contributes in bearing part of the tensile force at tension zone of specimen; 3) Third stage (B–D): this stage consists of two segments: non-linear segment (B-C) and linear segment (C-D).

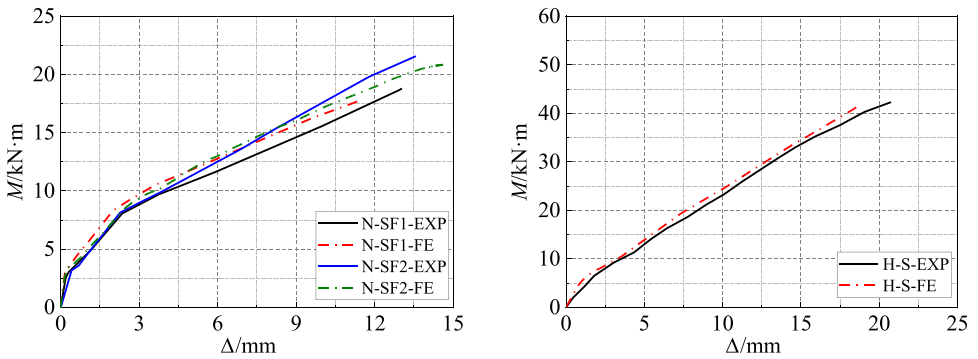

Fig. 7. Comparison of moment-deflection curves.

Table 7
Comparison of moment capacities.

No.	$M_{c,Exp}$ (kN.m)	$M_{c;FE}$ (kN.m)	$M_{c,FE}/M_{c,Exp}$	$M_{y,Exp}$ (kN.m)	$M_{y,FE}$ (kN.m)	$M_{y,FE}/M_{y,Exp}$	$M_{u,Exp}$ (kN.m)	$M_{u,FE}$ (kN.m)	$M_{u,FE}/M_{u,Exp}$
N-SF1	3.2	3.0	0.94	8.1	8.2	1.01	18.9	17.9	0.95
N-SF2	3.2	2.57	0.81	8.0	8.1	1.01	21.6	20.8	0.96
H-S1	N/A	4.8	N/A	44.2	41.7	0.94	46.0	41.7	0.91
APE			0.12			0.03			0.06
SD			0.04			0.02			0.02

Table 8
Comparison of deflections.

No.	$\Delta_{c,Exp}$ (mm)	$\Delta_{c,FE}$ (mm)	$\Delta_{c,FE}/\Delta_{c,Exp}$	$\Delta_{y,Exp}$ (mm)	$\Delta_{y,FE}$ (mm)	$\Delta_{y,FE}/\Delta_{y,Exp}$	$\Delta_{u,Exp}$ (mm)	$\Delta_{u,FE}$ (mm)	$\Delta_{u,FE}/\Delta_{u,Exp}$
N-SF1	0.3	0.17	0.57	2.4	2.0	0.83	13.0	11.35	0.87
N-SF2	0.4	0.18	0.45	2.2	2.15	0.98	13.6	14.4	1.06
H-S1	N/A	0.85	N/A	20.9	18.7	0.90	N/A	N/A	N/A
APE			0.5			0.097			0.095
SD			0.06			0.06			0.035

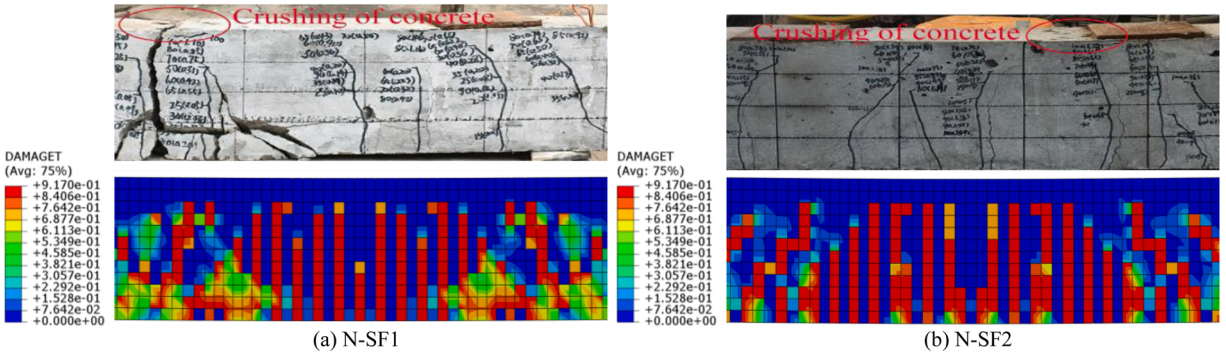

(a) N-SF1 (b) N-SF2

Fig. 8. Comparison of cracks pattern at failure.

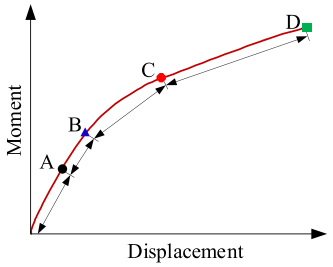

Fig. 9. Typical moment-deflection curve of SFCBs reinforced UHPC beams.

After UHPC reaches the peak tensile stress, its post-peak tensile stress gradually decreases, and thus the flexural stiffness of specimen gradually decreases until UHPC eventually quits working at tension zone of specimen, exhibiting a non-linear transition curve (B-C). Then followed by a linear response (C-D) until failure with good stiffness due to the stable secondary stiffness of SFCBs.

6. Parametric studies

Parametric study was carried out to investigate the effects of various parameters on the flexural behavior of SFCBs reinforced UHPC beams in terms of flexural stiffness, cracking, yielding and ultimate moment, cracking, yielding and ultimate deflection, deflection ductility ($u_\Delta = \Delta_u/\Delta_y$), and energy dissipation. The cracking moment refers to the moment when the tensile stress of UHPC reaches its peak point. The yield moment refers to the moment when the inner steel core of SFCBs reaches its yield strain. The ultimate moment refers to the moment when the compression concrete crushed or the tension SFCBs ruptured. The elastic energy dissipation (E_{el}) refers to the area under the moment-deflection curve up to the yielding point, and the total energy dissipation (E_d) refers to the area under the

moment-deflection curve up to failure.

In this section, the inner steel core area ratio to the total area of SFCB (α_s), the yield strength of the inner steel core (f_y); the reinforcement ratio (ρ); the ultimate strength (f_u) and the elastic modulus (E_f) of SFCB's outer FRP, and concrete type were the main parameters. When one of the parameters changed, the following parameters were kept constant: $\alpha_s = 0.25$, $f_y = 400$ MPa, $f_u = 1000$ MPa, $E_f = 50$ GPa, $\rho = 1.3\%$, and concrete type was UHPC. In addition, the mechanical properties of reinforcement bars were calculated by using Eq. (6), which was presented in the subsection 3.2.3. While the flexural stiffness of specimen can be calculated by Eq. (11) [56].

$$B = \frac{PL_s}{24\Delta}\left(3L_e^2 - 4L_s^2\right) \tag{11}$$

where B is the flexural stiffness of specimen, L_e ($3L_s$) is the effective span of specimen. The initial, second and third stiffness (B_1, B_2 and B_3) refer to the flexural stiffness of specimen at the first stage, second stage, and the linear segment of the third stages, respectively.

6.1. Inner steel area ratio

Fig. 10 shows the stress-strain curve of SFCBs with different inner steel area ratios.

In order to investigate the effect of the inner steel area ratio (α_s) to the total area of SFCB on flexural response of reinforced UHPC beams, five FE models were established with five different α_s from 0.0 to 1.0. Where $\alpha_s = 0.0$ represents FRP bar, and $\alpha_s = 1.0$ represents steel bar, while α_s of 0.25, 0.44 and 0.7 represent the inner steel area ratio of steel bar diameter of 6, 8 and 10 mm respectively, to the total area of SFCB with diameter of 12 mm. According to the analysis results, the maximum moment capacity of each specimen was determined by the SFCBs rupture, which refers to a tension failure. While the analysis process for steel-reinforced UHPC beam specimen continued until the concrete crushing.

Fig. 11-a shows the moment-deflection curves. As expected, with the increase of α_s, the flexural stiffness of SFCBs reinforced UHPC specimens significantly increases in the elastic stage of moment-deflection curve due to the increase in the elastic modulus of SFCB. In the second stage, although SFCBs reach its yielding strain and the stiffness of SFCBs decreases, the flexural stiffness of specimen slightly decreases due to the contributing of UHPC in bearing part of the tensile force at the tension zone of specimen. In the third stage, the flexural stiffness of specimen decreases with the increasing of α_s. This is because the post-yield stiffness of SFCBs decreases with the increase of α_s. For the reinforced specimen with steel bars (α_s =1.0), when UHPC reaches the peak tensile stress, the flexural stiffness of the specimen gradually decreases until the peak load, followed by a drop in the moment capacity, after that, the moment capacity slightly decreases with the increase of the deflection.

From Fig. 11b–d, with the increase of inner steel area ratio (α_s), the cracking moment, yield moment, and yield deflection significantly increase, while the cracking deflection almost not change, but the ultimate moment and corresponding deflection decrease with the increase of α_s, then the ductility and energy dissipation significantly decrease accordingly. This is because the elastic modulus and yield strength of SFCB increase with the increase of inner steel area ratio, but the secondary stiffness and ultimate strength decrease as shown in Fig. 10. For specimens failed by concrete crushing, the ultimate moment increases with the increase of α_s. This view is supported by Ge et al. [23], that the moment capacity of specimen reinforced with SFCBs (α_s =0.44) is larger than that of counterpart reinforced with BFRP bars (α_s =0.0). In addition, Sun et al. [24] found that when the specimen occurred the SFCB rupturing failure, the ultimate moment decreases with the increase of α_s, while the ultimate moment slightly decreases with the increase of α_s when the specimen occurred concrete crushing failure.

The failure type and the effect of inner steel ratio on ultimate moment, stiffness and energy dissipation are listed in Table 9. It can be seen that the initial stiffness increased by 62%, and the ultimate moment and total energy dissipation decreased by 37% and 77%, respectively, when α_s increased from 0.0 to 1.0. The flexural stiffness of third stage decreased by 9% when α_s increased from 0.0 to 0.7, and the elastic energy dissipation increased by 83% when α_s increased from 0.25 to 1.0. It was also found that the cracking moment,

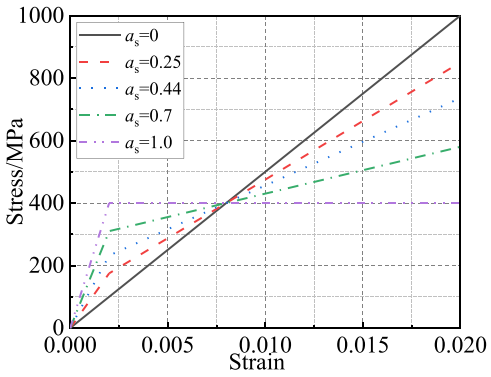

Fig. 10. Nominal stress-strain relationship of SFCBs.

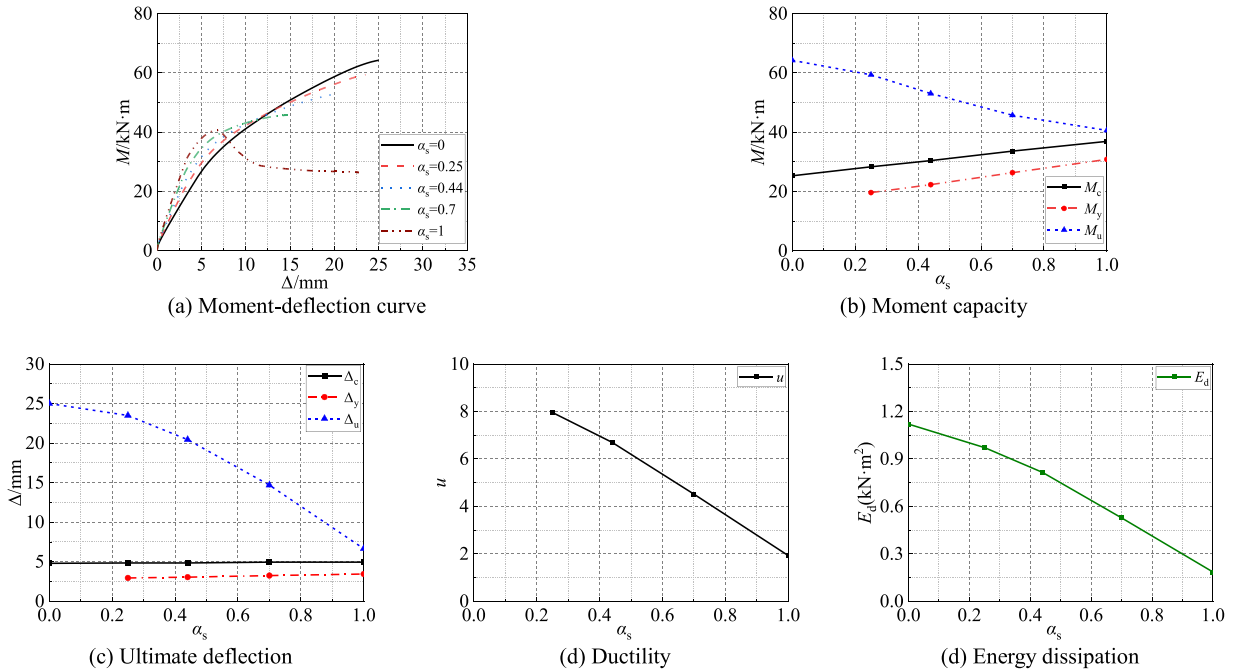

Fig. 11. Effect of inner steel area ratio.

Table 9
Failure type and effect of inner steel ratio on ultimate moment, stiffness and energy dissipation.

α_s	M_u (kN.m)	$M_{u,i}/M_{u,\alpha s=0.0}$	B_1 (kN.m^2)	B_2 (kN.m^2)	B_3 (kN.m^2)	E_{el} (kN.m^2)	E_d (kN.m^2)	Failure type
0.0	64.3	1.00	1023.3	1023.3	664.0	0.061	1.07	Tension
0.25	59.4	0.92	1292.8	1134.2	655.8	0.029	0.97	Tension
0.44	53.1	0.83	1421.2	1217.9	639.4	0.034	0.79	Tension
0.7	45.7	0.71	1574.5	1318.6	604.0	0.043	0.51	Tension
1.0	40.6	0.63	1734.7	1447.3	362.6	0.053	0.24	Tension

yield moment, and yield deflection increased by 46%, 87% and 21%, respectively, when α_s increased from 0.0 to 1.0, while the ultimate deflection and ductility decreased by 72% and 76%, respectively.

6.2. *Yield strength of inner steel core*

In order to investigate the effect of yield strength of inner steel core on the flexural response of UHPC beams reinforced with SFCBs, four FE models were built with four yield strengths of inner steel, that is 300, 400, 500 and 600 MPa. According to the analysis results, the maximum moment capacity of each specimen was determined by the SFCBs rupture, which refers to a tension failure.

Fig. 12 shows the comparison of predicted results, it can be observed that the yield strength of inner steel core has slight effect on the flexural stiffness, ultimate moment and the energy dissipation, and has no effect on the cracking moment and deflection as well as the ultimate deflection. The yield strength of inner steel core has a significant effect on the yield moment, deflection and ductility. With the increase of yield strength of inner steel core, the yield moment and yield deflection significantly increase, and the energy dissipation and the ultimate moment slightly increase, but the ductility decreases due to the increment of yield deflection.

The failure type and the effect of yield strength of inner steel core on ultimate moment, stiffness and energy dissipation are listed in Table 10. It can be seen that, when the yield strength of inner steel core increased by 100% (from 300 to 600 MPa), the ultimate moment capacity and the stiffness of third stage only increased by 5%, and the second stiffness, and total energy dissipation increased by 9% and 12%, respectively. This can be attributed to the small inner steel area ratio (α_s =0.25) and the enhanced tensile behavior of UHPC, leading to the small effect of yield strength of inner steel core on the flexural performance of specimen. It was also found that yield moment and corresponding deflection increased by 89% and 111%, respectively, while the elastic energy dissipation increased by 300%, and the ductility decreased by 53% due to the increment of yield moment and yield deflection.

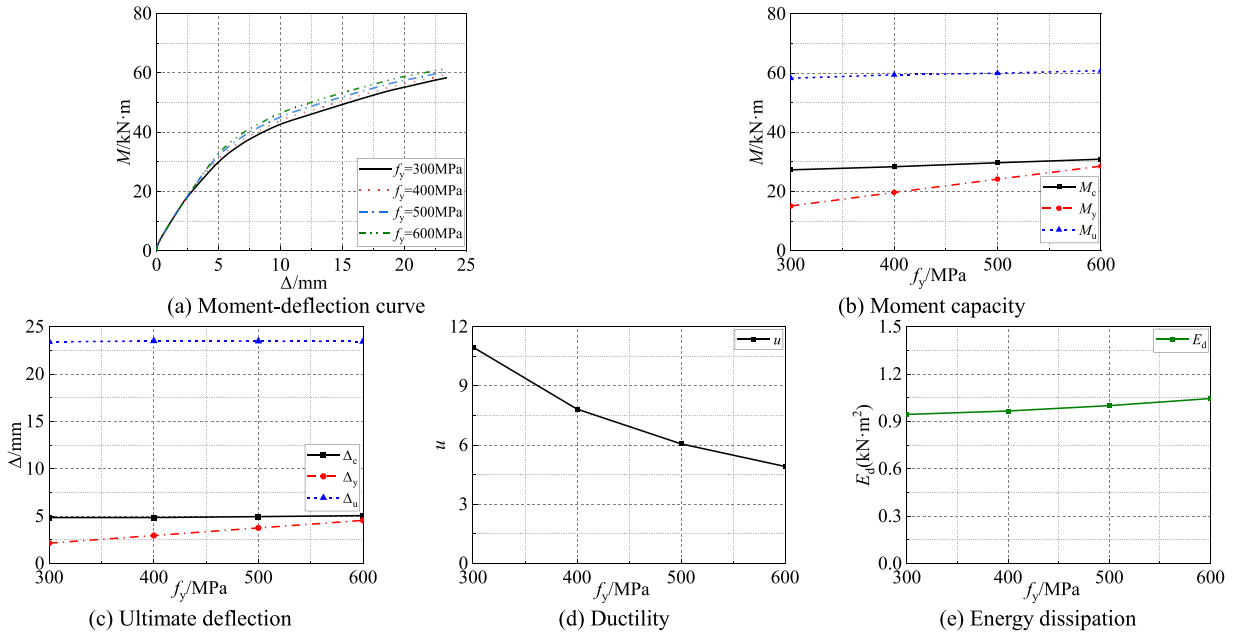

Fig. 12. Effect of yield strength of inner steel core.

Table 10
Failure type and effect of yield strength of inner steel core on ultimate moment, stiffness and energy dissipation.

f_y (MPa)	M_u (kN.m)	$M_{u,i}/M_{u,\ f_y=300}$	B_1 (kN.m^2)	B_2 (kN.m^2)	B_3 (kN.m^2)	E_{el} (kN.m^2)	E_d (kN.m^2)	Failure type
300	58.3	1.00	1358.9	1092.0	646.0	0.016	0.94	Tension
400	59.4	1.02	1358.9	1134.2	655.8	0.029	0.97	Tension
500	60.5	1.04	1358.9	1163.7	667.7	0.045	1.00	Tension
600	61.5	1.05	1358.9	1186.9	680.4	0.065	1.05	Tension

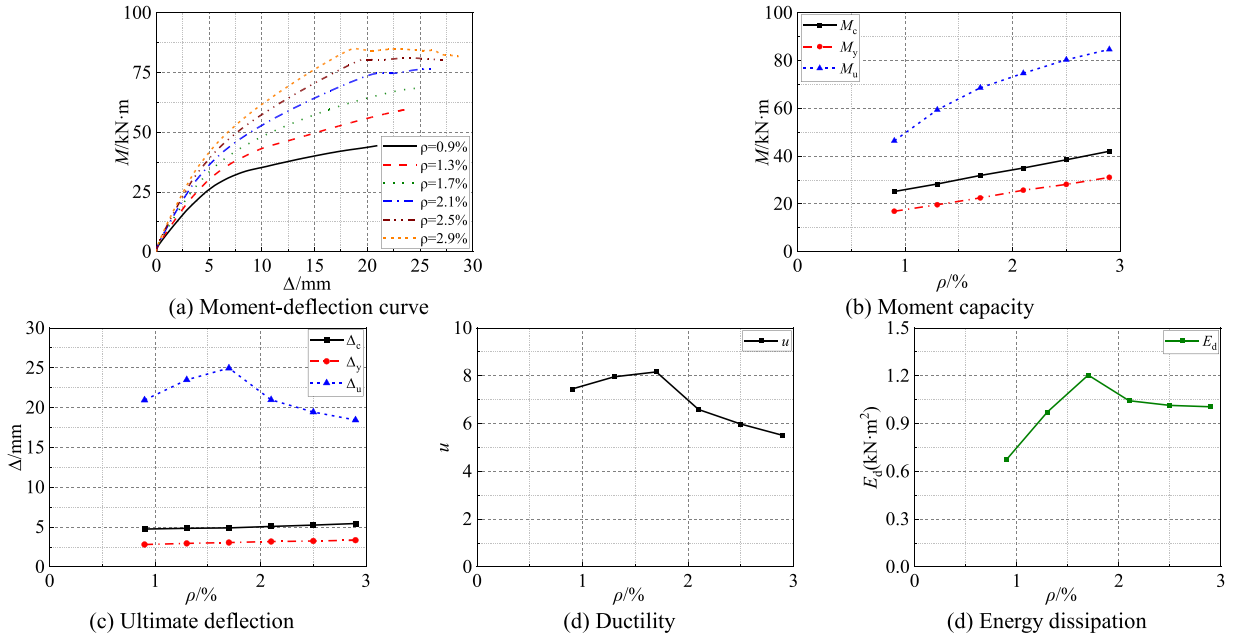

Fig. 13. Effect of the reinforcement ratio.

6.3. Reinforcement ratio

In order to investigate the effect of reinforcement ratio (ρ) on the flexural performance of UHPC beams reinforced with SFCBs, six FE models were established with varied reinforcement ratios from 0.9% to 2.9% having a increment of 0.4%. According to the analysis results, the maximum moment capacities of the specimens with reinforcement ratios of 0.9%, 1.3% and 1.7% were determined by the SFCBs rupture, which refers to a tension failure. While the maximum moment capacities of the specimens with reinforcement ratios of 2.1, 2.5% and 2.9% were determined by the concrete crushing, which refers to a compression failure.

Fig. 13 shows a comparison of the predicted moment-deflection curves, moment capacity, deflection values, ductility and energy dissipation. It can be clearly observed that the flexural stiffness throughout the loading process is improved as the steel reinforcement ratio increases. With the increase of reinforcement ratio (ρ), the cracking and yield moment capacities increase linearly, while the ultimate moment increase non-linearly regardless the failure mode. It can be also observed that with the increase of reinforcement ratio (ρ), the ultimate deflection, ductility and total energy dissipation, firstly increase, then decrease when the failure mode changes from tension to compression.

The failure type and the effect of reinforcement ratio on ultimate moment, stiffness and energy dissipation are listed in Table 11. It can be seen that the ultimate moment capacity increased by 48%, when the reinforcement ratio (ρ) increased by 89% from 0.9% to 1.7%. When the failure mode changed from the tension to compression, the ultimate moment capacity only increased by 24%, when the reinforcement ratio (ρ) increased by 71% from 1.7% to 2.9%, indicating that the increment of ultimate moment is not proportional to the increment of reinforcement ratio. The initial stiffness, third stiffness and the elastic energy dissipation increased by 54%, 98% and 116%, respectively, when the reinforcement ratio (ρ) increased from 0.9% to 2.9%, while total energy dissipation firstly increased by 80% when the reinforcement ratio (ρ) increased from 0.9% to 1.7%, then decreased by 16% when the reinforcement ratio (ρ) increased from 2.1% to 2.9%. It was also found that the ultimate deflection and ductility, firstly increased by 20% and 9.5%, respectively, when the reinforcement ratio (ρ) increased from 0.9% to 1.7%, then decreased by 26% and 33%, respectively, when the reinforcement ratio (ρ) increased from 2.1% to 2.9%.

6.4. Ultimate strength of SFCB's outer FRP

In order to investigate the effect of ultimate strength of SFCB's outer FRP on flexural response of UHPC beams reinforced with SFCBs, six FE models were established with different ultimate strength of SFCB's outer FRP from 600 to 1600 MPa with constant elastic modulus of 50 GPa, which represent from GFRP to BFRP [18,58]. According to the analysis results, the maximum moment capacities of the specimens with ultimate strength from 600 to 1200 MPa were determined by the SFCBs rupture, which refers to a tension failure. While the maximum moment capacities of the specimens with ultimate strength of 1400 and 1600 MPa were determined by the concrete crushing, which refers to a compression failure.

As observed from Fig. 14, the ultimate strength of SFCB's outer FRP has no effect on the flexural stiffness, cracking and yield moment and corresponding deflection, where the overall trend of flexural behavior of all specimens is the same. The ultimate moment and corresponding deflection, ductility and energy dissipation increase with the increase of the ultimate strength of SFCB's outer FRP when the specimen fails by tension failure. When the failure mode of specimen is the compression failure, the ultimate tensile strength of SFCB's outer FRP has no effect on flexural performance of specimen throughout the whole loading process. Sun et al. [24] reported that the significant decrease in curvature and ultimate moment of RC specimen reinforced with SFCBs was attributed to a decrease in the tensile strain of SFCB at the ultimate point when the failure mode of specimen was the rupture of SFCBs. While the ultimate moment and curvature were equivalent when the failure mode of specimen was concrete crushing. In addition, Ge et al. [23,57] found that the ultimate strength of FRP has no effect on the deflection or moment capacity when the failure mode of specimen is concrete crushing.

The failure type and the effect of ultimate strength of outer FRP on ultimate moment, stiffness and energy dissipation are listed in Table 12. It can be seen that the ultimate moment and total energy dissipation increased by 28% and 180%, respectively, when the ultimate strength of SFCB's outer FRP increased by 100% from 600 to 1200 MPa, when the failure mode was the rupture of SFCBs. In addition, there is no change in the initial stiffness, third stiffness and elastic energy dissipation. It was also found that both the ultimate deflection and ductility increased by 100% when the ultimate strength of SFCB's outer FRP increased from 600 to 1200 MPa. When the ultimate strength of SFCB's outer FRP increased from 1400 to 1600 MPa, the failure mode of specimen was concrete crushing, and the overall flexural performance, in terms of the stiffness, moment capacity, deflection value, ductility and energy dissipation, was unchanged.

6.5. Elastic modulus of SFCB's outer FRP

In order to investigate the effect of the elastic modulus of SFCB's outer FRP on the flexural performance of UHPC beams reinforced with SFCBs, four FE models were built with varied elastic modulus of SFCB's outer FRP from 30 to 100 GPa with constant ultimate tensile strength of 1000 MPa, which represent from GFRP to BFRP [24,58]. Fig. 16 shows the stress-strain curve of SFCBs with different elastic modulus of SFCB's outer FRP. According to the analysis results, the maximum moment capacity of each specimen was determined by the SFCBs rupture, which refers to a tension failure.

Fig. 16 demonstrates that with the increase of the elastic modulus of SFCB's outer FRP, the flexural stiffness and the moment capacity increase significantly throughout the loading process. However, the increase rate of moment capacity decreases gradually, meanwhile the ultimate deflection, ductility and energy dissipation significantly decrease. Fig. 16 also shows that the elastic modulus

Table 11
Failure type and effect of reinforcement ratio on ultimate moment, stiffness and energy dissipation.

ρ (%)	M_u (kN.m)	$M_{u,i}/M_{u,\rho=0.9\%}$	B_1 (kN.m^2)	B_2 (kN.m^2)	B_3 (kN.m^2)	E_{el} (kN.m^2)	E_d (kN.m^2)	Failure type
0.9	46.4	1.00	1168.8	1029.3	449.5	0.024	0.67	Tension
1.3	59.4	1.28	1292.8	1134.2	567.3	0.029	0.97	Tension
1.7	68.6	1.48	1428.9	1263.9	656.4	0.034	1.20	Tension
2.1	74.7	1.61	1568.2	1337.6	746.4	0.041	1.04	Compression
2.5	80.4	1.73	1682.0	1422.1	825.5	0.046	1.01	Compression
2.9	84.8	1.82	1801.5	1497.1	891.1	0.052	1.01	Compression

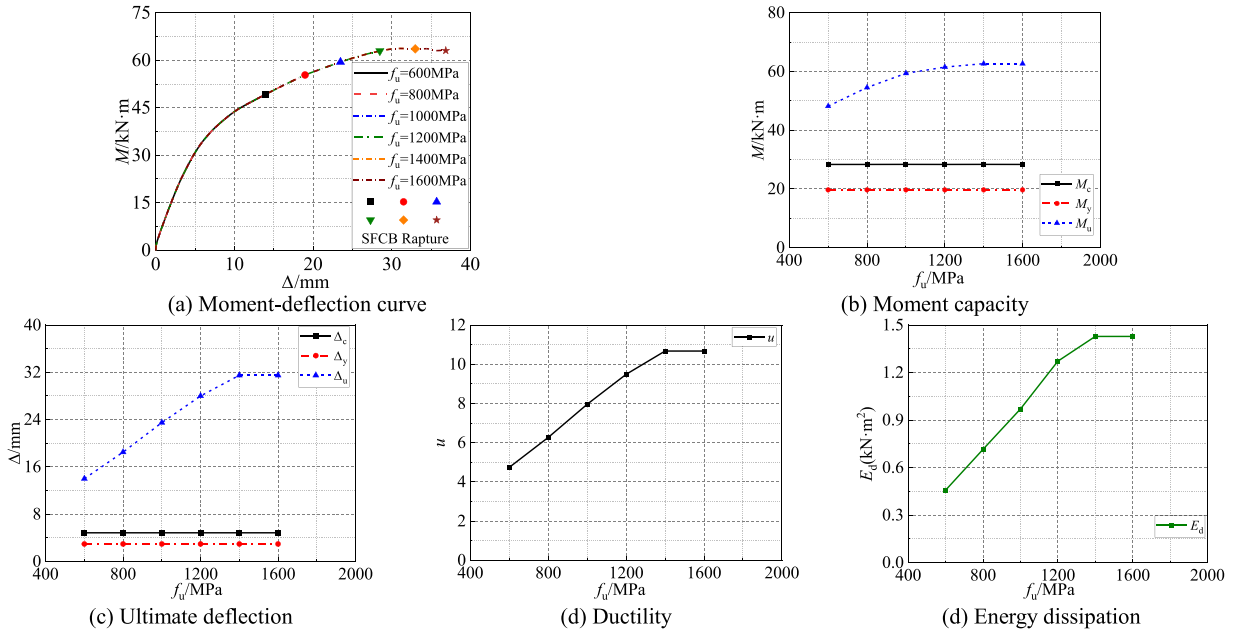

Fig. 14. Effect of ultimate strength of SFCB's outer FRP.

Table 12
Failure type and effect of ultimate strength of outer FRP on ultimate moment, stiffness and energy dissipation.

f_u (MPa)	M_u (kN.m)	$M_{u,i}/M_{u,\ fu=600}$	B_1 (kN.m^2)	B_2 (kN.m^2)	B_3 (kN.m^2)	E_{el} (kN.m^2)	E_d (kN.m^2)	Failure type
600	48.2	1.00	1292.8	1133.3	667.3	0.03	0.46	Tension
800	54.5	1.13	1292.8	1133.3	667.3	0.03	0.72	Tension
1000	59.4	1.23	1292.8	1133.3	667.3	0.03	0.97	Tension
1200	61.5	1.28	1292.8	1133.3	667.3	0.03	1.27	Tension
1400	62.7	1.30	1292.8	1133.3	667.3	0.03	1.43	Compression
1600	62.7	1.30	1292.8	1133.3	667.3	0.03	1.43	Compression

of SFCB's outer FRP has no obvious effect on the yield and cracking deflections. The ultimate deflection significantly decreases due to the decrement of ultimate tensile strain of SFCB as shown in Fig. 15, which also leads to the decrease in the ductility and the energy dissipation accordingly. It is also observed from Fig. 16 that the moment capacity and flexural stiffness increase, while the ultimate deflection decreases nonlinearly with the increase of elastic modulus of SFCB's outer FRP.

The failure type and the effect of elastic modulus of outer FRP on ultimate moment, stiffness and energy dissipation are listed in Table 13. It can be seen that the ultimate moment, initial stiffness, third stiffness and elastic energy dissipation increased by 24%, 19%, 56% and 42%, respectively, when the elastic modulus of SFCB's outer FRP increased from 30 to 100 GPa, whereas the total energy dissipation decreased by 56%. It was also found that the ultimate deflection and ductility decreased by 54% and 60%.

6.6. Strength and type of concrete

In order to investigate the effect of strength and type of concrete on the flexural performance of beam reinforced with SFCBs, three FE models were created with varied concrete strengths and types (NSC, HSC and UHPC). According to the analysis results, the maximum moment capacities of the reinforced UHPC specimen was determined by the SFCBs rupture, which refers to a tension failure.

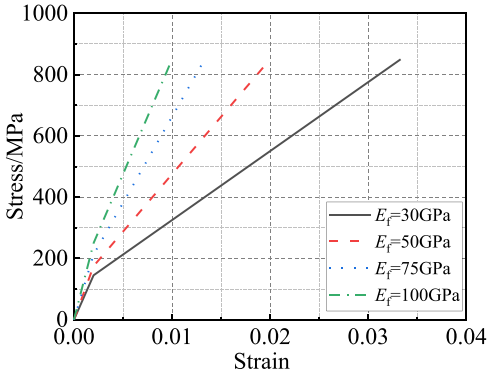

Fig. 15. Nominal stress-strain relationship of SFCBs.

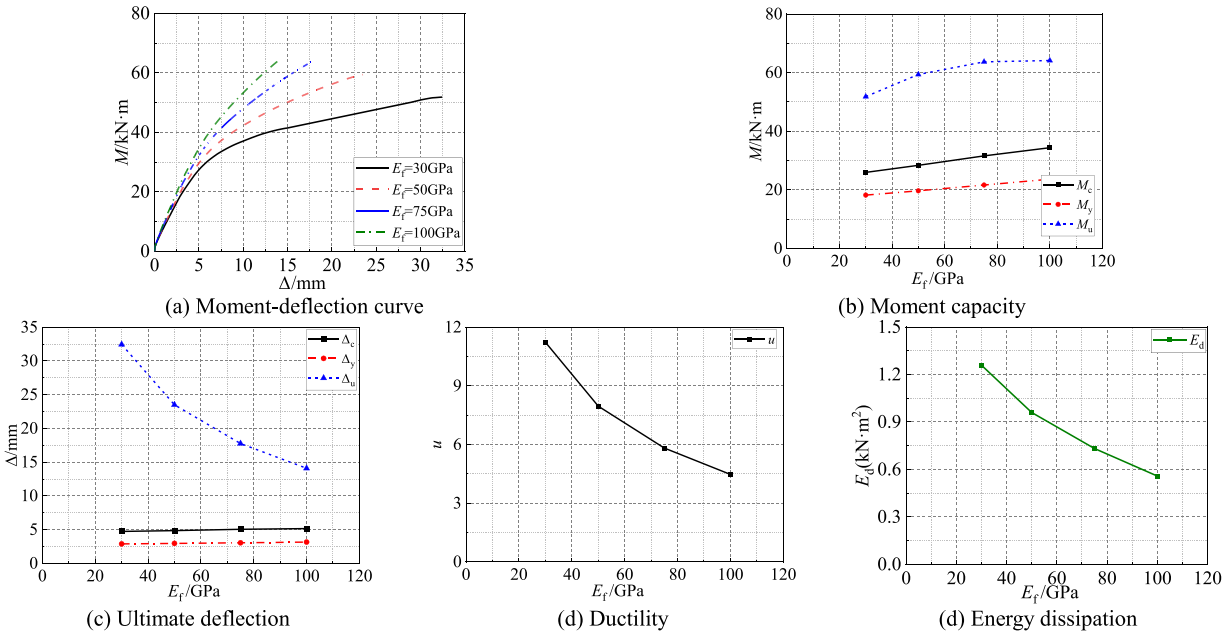

Fig. 16. Effect of elastic modulus of SFCB's outer FRP.

Table 13
Failure type and effect of elastic modulus of outer FRP on ultimate moment, stiffness and energy dissipation.

E_f (GPa)	M_u (kN.m)	$M_{u,i}/M_{u,\ Ef\ =\ 30}$	B_1 (kN.m^2)	B_2 (kN.m^2)	B_3 (kN.m^2)	E_{el} (kN.m^2)	E_d (kN.m^2)	Failure type
30	51.8	1.00	1222.3	1063.8	565.3	0.026	1.30	Tension
50	59.4	1.15	1292.8	1134.2	673.8	0.029	0.97	Tension
75	63.7	1.23	1375.5	1212.9	786.1	0.033	0.76	Tension
100	64.1	1.24	1453.6	1294.7	882.8	0.037	0.58	Tension

While the maximum moment capacities of the reinforced NSC and HSC specimens were determined by the concrete crushing, which refers to a compression failure.

Fig. 17 demonstrates that the trend of moment-deflection curves for SFCBs reinforced NSC and HSC specimens were similar. These curves presented three stages with two inflection points throughout the loading process, namely: first stage (elastic stage), from initial loading to concrete cracking; second stage (post-cracking stage), form concrete cracking to SFCB yielding; and third stage (post-yielding stage), from SFCB yielding to failure. Fig. 17 also shows that with increasing the concrete strength, the cracking and ultimate moment capacities, and the ultimate deflection significantly increase. Thus, the ductility and energy dissipation increase. On the other hand, the trend of moment-deflection curve for SFCBs reinforced UHPC was different as compared to that of SFCBs reinforced NSC and HSC, and presented three stages without inflection points as previously described in Section 5. In addition, the moment capacities,

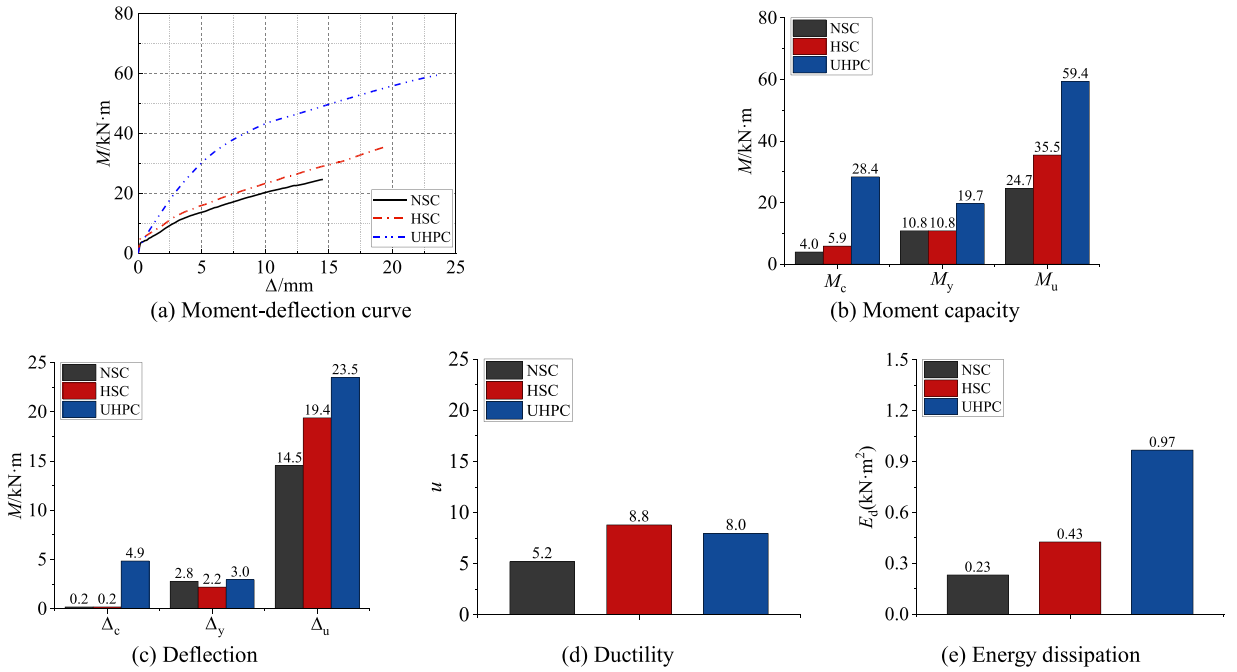

Fig. 17. Effect of concrete type.

Table 14
Failure type and effect of strength and type of concrete on ultimate moment, stiffness and energy dissipation.

Concrete type	M_u (kN.m)	$M_{u,i}/M_{u,NSC}$	B_1 (kN.m^2)	B_2 (kN.m^2)	B_3 (kN.m^2)	E_{el} (kN.m^2)	E_d (kN.m^2)	Failure type
NSC	24.7	1.00	4094.6	751.4	328.9	0.0004	0.23	Compression
HSC	35.5	1.44	6088.7	953.8	388.6	0.0006	0.43	Compression
UHPC	59.4	2.41	1292.8	1134.2	659.8	0.029	0.97	Tension

flexural stiffness and the energy dissipation of reinforced UHPC were significantly improved as compared to those of NSC and HSC counterparts. This is attributed to the high tensile strength and its enhanced post-cracking behavior of UHPC.

The failure type and the effect of strength and type of concrete on ultimate moment, stiffness and energy dissipation are listed in Table 14. It can be seen that the SFCBs reinforced NSC and HSC specimens exhibited higher initial stiffness as compared to that of UHPC counterpart. While the second and third stiffness of SFCBs reinforced UHPC beam were two times those of NSC counterpart, indicating the effectiveness of enhanced post-peak tensile strength of UHPC in limiting the increase rate of deflection and improving the flexural stiffness. However, the low initial stiffness and the improved second and third stiffness of UHPC led to large yield deflection and low ductility of SFCB reinforced UHPC when compared to those of HSC counterpart. The elastic energy dissipation of reinforced NSC and HSC specimens were extremely slight as compared to that of UHPC counterpart, and the total energy dissipation of SFCB-reinforced UHPC was about 4.2 and 2.2 times, respectively, that of SFCBs reinforced NSC and HSC counterparts.

As can be seen from Fig. 17, the yield moment capacity of SFCB-reinforced UHPC specimen increased only by about 82% when compared to that of SFCB reinforced NSC and HSC counterparts. While the cracking moment capacity was about 7.1 and 4.8 times, respectively, that of NSC and HSC counterparts. Furthermore, although the failure type of UHPC specimen was the SFCBs rupture, and the failure type of HSC and NSC specimens was the concrete crushing, the ultimate moment capacity of UHPC specimen was about 2.4 and 1.7 times, respectively, that of NSC and HSC counterparts. Overall, the enhancement in the tensile and compression performance of UHPC significantly improved the flexural performance of SFCBs reinforced UHPC specimen in terms of flexural stiffness, moment capacity, deflection, ductility and energy dissipation.

7. Conclusion

Parametric studies were conducted to investigate the effects of various parameters on the flexural performance of UHPC beams reinforced with SFCBs. The observations and conclusions could be summarized as follows.

1) The FE models well predict the flexural behavior of reinforced NSC and HSC beams in terms of moment-deflection curve, moment capacity, deflection, cracks pattern and failure mode. The moment capacity and its corresponding deflection were consistent with

the test results with an average percentage error of 7.0% and 9.6%, respectively, illustrating the validity of the developed models to predict the flexural behavior of reinforced NSC and HSC beams.

2) With the increase of area ratio of inner steel to SFCB, the flexural stiffness, moment capacity and elastic energy dissipation of SFCBs reinforced UHPC beams are significantly improved up to the peak tensile strength point of UHPC. However, the ultimate moment and corresponding deflection decreased significantly. Thus, the ductility and the total energy dissipation decrease correspondingly.
3) With the increase of the yield strength of inner steel, the yield moment and corresponding deflection significantly increase. The effect on the flexural stiffness, energy dissipation and ultimate moment is slight, and that has no effect on cracking and ultimate deflection.
4) With the increase of reinforcement ratio, the flexural stiffness, elastic energy dissipation and moment capacity significantly increase. While the ultimate deflection, ductility and total energy dissipation, firstly increase, then decrease when the failure mode of specimen changes from tension failure to compression failure.
5) With the increase of ultimate strength of SFCB's outer FRP, only the ultimate moment and corresponding deflection increase when the failure mode is the rupture of SFCBs, leading to the increasing of ductility and total energy dissipation. However, when the failure mode of specimen is compression failure, there is no effect of ultimate strength of out-wrapped FRP on overall flexural performance of specimen.
6) With the increase of elastic modulus of SFCB's outer FRP, the flexural stiffness, elastic energy dissipation and moment capacity increase gradually. However, the increase rate of moment capacity significantly decreases. In addition, the ultimate deflection significantly decreases due to the decrease of tensile strain of SFCB. Thus, the ductility and total energy dissipation decrease accordingly.
7) The SFCB-reinforced UHPC specimen presents different flexural response when compared to that of reinforced NSC and HSC counterparts. There were no inflection points on the moment-deflection curve, where the post-cracking stiffness gradually decreases with the increase of the applied load, even the reinforcement bars reaches its yield strength. In addition, the flexural stiffness and moment capacity of SFCB-reinforced UHPC specimen at the ultimate point were 2.0 and 2.4 times, respectively, those of reinforced NSC counterpart. The enhancement of tensile and compression performance of UHPC exhibit a significant effect on the flexural performance of reinforced UHPC specimen in terms of flexural stiffness, moment capacity, ductility and energy dissipation.

Declaration of Competing Interest

The authors declare that they have no known competing financial interests or personal relationships that could have appeared to influence the work reported in this paper.

Acknowledgements

The authors would like to acknowledge the financial support to the work by the Natural Science Foundation of Jiangsu Province, China (BK20201436), the China Postdoctoral Science Foundation (2018M642335), the Science and Technology Project of Jiangsu Construction System, China (2018ZD047, 2021ZD06), the Science and Technology Project of Gansu Construction System, China (JK2021-19), the National Natural Science Foundation of China (51678514), the Science and Technology Innovation Fund of Yangzhou University, China (2020-65), the Open Foundation of Jiangsu Province Engineering Research Center of Prefabricated Building and Intelligent Construction, China (2021), the Science and Technology Cooperation Fund Project of Yangzhou City and Yangzhou University, China (YZU212105), the Practice and Innovation Plan for Postgraduates in Jiangsu Province, China (SJCX21_1589), the Blue Project Youth Academic Leader of Colleges and Universities in Jiangsu Province, China (2020) and the Deputy General Manager Science and Technology Project of Jiangsu Province, China (FZ20200869).

References

[1] J. Qi, J. Wang, Z. Ma, Flexural response of high- strength steel- ultra- high- performance fibre reinforced concrete beams based on a mesoscale constitutive model: Experiment and theory, Struct. Concr. 19 (3) (2018) 719–734.
[2] S. Aldabagh, F. Abed, S. Yehia, Effect of types of concrete on flexural behavior of beams reinforced with high-strength steel bars, J. ACI Struct. 115 (2) (2018) 351–364.
[3] F. Abed, A.R. Alhafiz, Effect of basalt fibers on the flexural behavior of concrete beams reinforced with BFRP bars, Compos. Struct. 215 (2019) 23–34.
[4] F. Bulavs, I. Radinsh, N. Tirans, Improvement of capacity in bending by the use of FRP layers on RC beams, J. Civ. Eng. Manag. 11 (3) (2005) 169–174.
[5] T.A. El-Sayed, Y.A. Algash, Flexural behavior of ultra-high performance geopolymer RC beams reinforced with GFRP bars, Case Stud. Constr. Mater. 15 (2021), e00604.
[6] P. Zhang, J. Shang, Y. Liu, J. Shao, D. Gao, Z. Dong, S.A. Sheikh, Flexural behavior of GFRP bar-reinforced concrete beams with U-shaped UHPC stay-in-place formworks, J. Build. Eng. 45 (2022), 103403.
[7] R.Z. Al-Rousan, Failure analysis of polypropylene fiber reinforced concrete two-way slabs subjected to static and impact load induced by free falling mass, Lat. Am. J. Sol. Struct. 15 (2018).
[8] Z. Zhang, E.M. Abbas, Y. Wang, et al., Experimental study on flexural behavior of the BFRC-concrete composite beams, Case Stud. Constr. Mater. 15 (2021), e00738.
[9] R. Al-Rousan, Influence of polypropylene fibers on the flexural behavior of reinforced concrete slabs with different opening shapes and sizes, Struct. Concr. 18 (6) (2017) 986–999.
[10] D.Y. Yoo, Y.S. Yoon, Structural performance of ultra-high-performance concrete beams with different steel fibers, Eng. Struct. 102 (2015) 409–423.
[11] H.O. Shin, K. Kim, T. Oh, D.Y. Yoo, Effects of fiber type and specimen thickness on flexural behavior of ultra-high-performance fiber-reinforced concrete subjected to uniaxial and biaxial stresses, Case Stud. Constr. Mater. 15 (2021), e00726.

[12] M. Alhassan, R. Al-Rousan, A. Ababneh, Flexural behavior of lightweight concrete beams encompassing various dosages of macro synthetic fibers and steel ratios, Case Stud. Constr. Mater. (2017) 280–293.
[13] A. Ababneh, R. Al-Rousan, M. Alhassan, M. Alqadami, Influence of synthetic fibers on the shear behavior of lightweight concrete beams, Adv. Struct. Eng. 20 (11) (2017) 1671–1683.
[14] R.Z. Al-Rousan, Behavior of macro synthetic fiber concrete beams strengthened with different CFRP composite configurations, J. Build. Eng. 20 (2018) 595–608.
[15] R.Z. Al-Rousan, M.A. Alhassan, E.A. AlShuqari, Behavior of plain concrete beams with DSSF strengthened in flexure with anchored CFRP sheets—Effects of DSSF content on the bonding length of CFRP sheets, Case Stud. Constr. Mater. 9 (2018), e00195.
[16] G. Wu, Z.S. Wu, Y.B. Luo, Z.Y. Sun, X.Q. Hu, Mechanical properties of steel-FRP composite bar under uniaxial and cyclic tensile loads, J. Mater. Civ. Eng. 22 (10) (2010) 1056–1066.
[17] Y. Tang, Z. Sun, G. Wu, Compressive behavior of sustainable steel-FRP composite bars with different slenderness ratios, Sustainability 11 (4) (2019) 1118.
[18] Z. Sun, Y. Tang, Y. Luo, G. Wu, X. He, Mechanical properties of steel-FRP composite bars under tensile and compressive loading, Int. J. Polym. Sci. (2017), 5691278.
[19] Y. Zhou, X. Zheng, F. Xing, L. Sui, Y. Zheng, X. Huang, Investigation on the electrochemical and mechanical performance of CFRP and steel-fiber composite bar used for impressed current cathodic protection anode, Constr. Build. Mater. 255 (2020) 119–377.
[20] D. Zhao, J. Pan, Y. Zhou, L. Sui, Z. Ye, New types of steel-FRP composite bar with round steel bar inner core: Mechanical properties and bonding performances in concrete, Constr. Build. Mater. 242 (2020), 118062.
[21] Z. Dong, G. Wu, Y. Xu, Experimental study on the bond durability between steel-FRP composite bars (SFCBs) and sea sand concrete in ocean environment, Constr. Build. Mater. 115 (2016) 277–284.
[22] G. Wu, Z.Y. Sun, Z.S. Wu, Y.B. Luo, Mechanical properties of steel-FRP composite bars (SFCBs) and performance of SFCB reinforced concrete structures, Adv. Struct. Eng. 15 (4) (2012) 625–635.
[23] W. Ge, Y. Wang, A. Ashour, W. Lu, D. Cao, Flexural performance of concrete beams reinforced with steel–FRP composite bars, Arch. Civ. Mech. Eng. 20 (2020), 56.
[24] Z. Sun, Y. Yang, W. Yan, G. Wu, X. He, Moment-curvature behaviors of concrete beams singly reinforced by steel-FRP composite bars, Adv. Civ. Eng. (2017), 1309629.
[25] L. Wang, Z. Song, C. Huang, L. Ma, F. Fu, Flexural capacity of steel-FCB bar-reinforced coral concrete beams, Struct. Concr. 21 (6) (2020) 2722–2735.
[26] L. Ding, M. Lei, X. Wang, Y. Shi, Z. Zhu, P. Yu, Z. Wu, Durability of concrete members reinforced with steel-FRP composite bars under dry-wet cycles of seawater, Structures 33 (5) (2021) 2273–2283.
[27] Y. Zhou, H. Gao, Z. Hu, Y. Qiu, M. Guo, X. Huang, B. Hu, Ductile, durable, and reliable alternative to FRP bars for reinforcing seawater sea-sand recycled concrete beams: steel/FRP composite bars, Constr. Build. Mater. 269 (2021), 121264.
[28] Z. Dong, G. Wu, X.L. Zhao, H. Zhu, J. Lian, Bond durability of steel-FRP composite bars embedded in seawater sea-sand concrete under constant bending and shearing stress, Constr. Build. Mater. 192 (2018) 808–817.
[29] L. Wang, N. Shen, M. Zhang, F. Fu, K. Qian, Bond performance of Steel-CFRP bar reinforced coral concrete beams, Constr. Build. Mater. 245 (2020) 118–456.
[30] K. Wille, A.E. Naaman, G.J. Parra-Montesinos, Ultra-high performance concrete with compressive strength exceeding 150 MPa (22 ksi): a simpler way, ACI Mater. J. 108 (1) (2011).
[31] S. Allena, C.M. Newtson, Ultra-high strength concrete mixtures using local materials, J. Civ. Eng. Arch. 5 (4) (2011) 322–330.
[32] I.H. Yang, C. Joh, B.S. Kim, Shear behavior of ultra-high-performance fibre-reinforced concrete beams without stirrups, Mag. Concr. Res. 64 (2012) 979–993.
[33] Y.L. Voo, W.K. Poon, S.J. Foster, Shear strength of steel fiber-reinforced ultrahigh-performance concrete beams without stirrups, J. Struct. Eng. 136 (11) (2010) 1393–1400.
[34] F. Baby, P. Marchand, F. Toutlemonde, Shear behavior of ultrahigh performance fiber-reinforced concrete beams. I: Experimental investigation, J. Struct. Eng. 140 (5) (2014), https://doi.org/10.1061/(ASCE)ST.1943-541X.0000907.
[35] M. Pourbaba, H. Sadaghian, A. Mirmiran, A comparative study of flexural and shear behavior of ultra-high-performance fiber-reinforced concrete beams, Adv. Struct. Eng. 22 (7) (2019) 1727–1738.
[36] M.M. Ridha, I.N.T. Al-Shafi', M.M. Hasan, Ultra-high performance steel fibers concrete corbels: Experimental investigation, Case Stud. Constr. Mater. 7 (2017) 180–190.
[37] P. Zhang, X. Lv, Y. Liu, X. Zou, Y. Li, J. Wang, S.A. Sheikh, Novel fiber reinforced polymers (FRP)-ultrahigh performance concrete (UHPC) hybrid beams with improved shear performance, Constr. Build. Mater. 286 (2021), 122720.
[38] H. Yin, K. Shirai, W. Teo, Prediction of shear capacity of UHPC–concrete composite structural members based on existing codes, J. Civ. Eng. Manag. 24 (8) (2018) 607–618.
[39] G. Girovi, V. Radonjanin, M. Trivuni, D. Nikoli, Optimization of UHPFRC beams subjected to bending using genetic algorithms, J. Civ. Eng. Manag. 20 (4) (2014) 527–536.
[40] E. Ferrier, L. Michel, B. Zuber, G. Chanvillard, Mechanical behaviour of ultra-high-performance short-fibre-reinforced concrete beams with internal fibre reinforced polymer bars, Comp. Part B: Eng. 68 (2015) 246–258.
[41] D.Y. Yoo, N. Banthia, Y.S. Yoon, Flexural behavior of ultra-high-performance fiber-reinforced concrete beams reinforced with GFRP and steel rebars, Eng. Struct. 111 (2016) 246–262.
[42] Y. Zhang, Simplified method for evaluating the behavior of strain hardening cementitious composite flexural strengthening reinforced concrete members, Eng. Fract. Mech. 121 (2014) 11–27.
[43] M. Hafezolghorani, F. Hejazi, R. Vaghei, M.S.B. Jaafar, K. Karimzade, Simplified damage plasticity model for concrete, Struct. Eng. Int. 27 (1) (2017) 68–78.
[44] M. Alhassan, R.Z. Al-Rousan, L.K. Amaireh, M.H. Barfed, Nonlinear finite element analysis of BC connections: influence of the column axial load, jacket thickness, and fiber dosage, Structures 16 (2018) 50–62.
[45] R.Z. Al-Rousan, Empirical and NLFEA prediction of bond-slip behavior between DSSF concrete and anchored CFRP composites, Constr. Build. Mater. 169 (2018) 530–542.
[46] Y. Zhang, N. Ueda, H. Nakamura, M. Kunieda, Behavior investigation of reinforced concrete members with flexural strengthening using strain-hardening cementitious composite, ACI Struct. J. 114 (2) (2017) 417.
[47] R. Solhmirzaei, V. Kodur, Modeling the response of ultra-high performance fiber reinforced concrete beams. 6th International Workshop on Performance, Protection & Strengthening of Structures under Extreme Loading, PROTECT2017, Guangzhou (Canton), China.: Pro. Eng. 210 (2017) 211–219.
[48] M. Shafieifar, M. Farzad, A. Azizinamini, Experimental and numerical study on mechanical properties of ultra high performance concrete (UHPC), Constr. Build. Mater. 156 (2017) 402–411.
[49] D.T. Hashim, F. Hejazi, V.Y. Lei, Simplified constitutive and damage plasticity models for UHPFRC with different types of fiber, Int. J. Conc. Struct. Mater. 14 (2020), 45.
[50] M. Shafieifar, M. Farzad, A. Azizinamini, A comparison of existing analytical methods to predict the flexural capacity of Ultra High Performance Concrete (UHPC) beams, Constr. Build. Mater. 172 (2018) 10–18.

[51] A. Lapko, B. Sadowska- Buraczewska, A. Tomaszewicz, Experimental and numerical analysis of flexural composite beams with partial use of high strength/high performance concrete, J. Civ. Eng. Manag. 11 (2) (2005) 115–120.
[52] BSI Eur. 2: Des. Concr. Struct. (EN1992-1-1) 2005.
[53] B. Massicotte, A.E. Elwi, J.G. MacGregor, Tension stiffening model for planar reinforced concrete members, ASCE J. Struct. Eng. (1990) 3039–3058.
[54] ABAQUS Inc Abaqus Anal. User's Man. [M] 2010.
[55] T. Tysmans, M. Wozniak, O. Remy, J. Vantomme, Finite element modelling of the biaxial behavior of high performance fibre reinforced cement composites (HPFRCC) using Concrete Damaged Plasticity, Finite Elem. Anal. Des. 100 (2015) 47–53.
[56] S.W. Kim, K.H. Kim, Prediction of deflection of reinforced concrete beams considering shear effect, Materials 14 (2021) 6684.
[57] W. Ge, W. Song, A.F. Ashour, W. Lu, D. Cao, Flexural performance of FRP/steel hybrid reinforced engineered cementitious composite beams, J. Build. Eng. 31 (6) (2020), 101329.
[58] ACI Committee 440, Guide for the Design and Construction of Concrete Reinforced with FRP Bars, Amer. Concr. Inst., Farmington Hills, MI, 2015.